Inorg. Chem. **2002**, *41*, 4689–4699

Electronic Structure, Electrical and Magnetic Properties of RMo_8O_{14} Compounds (R = La, Ce, Pr, Nd, Sm) Containing Bicapped Mo_8 Clusters

Régis Gautier,*,†,‡ Ole Krogh Andersen,† Patrick Gougeon,*,§ Jean-François Halet,§ Enric Canadell,|| and James D. Martin⊥

Max-Planck-Institut für Festkörperforschung, Heisenbergstr. 1, D-70569 Stuttgart, Germany, Département de Physicochimie UPRES 1795, Ecole Nationale Supérieure de Chimie de Rennes, Institut de Chimie de Rennes, Campus de Beaulieu, F-35700 Rennes Cedex, France, Laboratoire de Chimie du Solide et Inorganique Moléculaire, UMR 6511 CNRS-Université de Rennes 1, Institut de Chimie de Rennes, Avenue du Général Leclerc, F-35042 Rennes Cedex, France, Institut de Ciència de Materials de Barcelona (CSIC), Campus de la Universitat Autònoma de Barcelona, 08193 Bellaterra, Spain, and Department of Chemistry, North Carolina State University, Raleigh, North Carolina 27695

Received March 12, 2002

Magnetic and electrical resistivity properties of RMo_8O_{14} (R = La, Ce, Pr, Nd, Sm) compounds containing different bicapped-octahedral Mo_8 clusters are discussed. Extended Hückel (EH) molecular calculations were carried out in order to study the influence of the position of metal capping atoms on the electronic structure of different Mo_8 isomers. Different optimal metal electron counts are possible for these clusters. Periodic density functional calculations confirm the molecular character of these compounds and allow the understanding of their semiconducting and magnetic properties.

Introduction

In solid-state chemistry, molybdenum is the transition metal which forms clusters with the largest variety of nuclearities and architectures. Thus, in ternary reduced molybdenum sulfides, selenides, and tellurides, Mo_3 triangles, Mo_4 tetrahedra, and Mo_6 octahedra have been characterized, for instance, in the compounds $K_2Mo_3Se_{18}$,[1] $GaMo_4X_8$ (X = S, Se, Te),[2] and $M_xMo_6X_8$ (M = 3d transition metal, alkaline, alkaline-earth or rare-earth metal, and so forth; X = S, Se, Te),[3] respectively. Larger clusters often result from the one-dimensional *trans*-face sharing of Mo_6 octahedra and have the general formula Mo_{3n}. Such condensed clusters are encountered, in particular, in the series of compounds $M_{n-2}Mo_{3n}X_{3n+2}$ (M = Rb, Cs; X = S, Se, Te; $n = 3-8$, 10, 12).[4] The final step of this face-sharing condensation is the infinite $|Mo_{6/2}|^1_\infty$ chain found in the quasi-one-dimensional compounds $M_2Mo_6X_6$ (M = Na, K, Rb, Cs; X = S, Se, or Te) and $AgMo_6Te_6$.[5]

In ternary and quaternary reduced molybdenum oxides, while similar triangular Mo_3 and octahedral Mo_6 units are

* To whom correspondence should be addressed. E-mail: rgautier@ensc-rennes.fr (R.G.); gougeon@univ-rennes1.fr (P.G.).
† Max-Planck-Institut für Festkörperforschung.
‡ Ecole Nationale Supérieure de Chimie de Rennes.
§ Université de Rennes 1.
|| Campus de la Universitat Autònoma de Barcelona.
⊥ North Carolina State University.

(1) Liao, J. H.; Kanatzidis, M. G. *Inorg. Chem.* **1992**, *31*, 431.
(2) Perrin, C.; Chevrel, R.; Sergent, M. *C. R. Acad. Sci.* **1975**, *280C*, 949.
(3) Chevrel, R.; Sergent, M. *Topics of Currents Physics*; Fischer, Ø., Maple, M. B., Eds.; Springer-Verlag: New York, 1982; p I25.
(4) (a) Gougeon, P. Ph.D. Thesis, University of Rennes, 1984. (b) Gougeon, P.; Potel, M.; Padiou, J.; Sergent, M. *Mater. Res. Bull.* **1987**, *22*, 1087. (c) Gougeon, P.; Potel, M.; Padiou, J.; Sergent, M. *Mater. Res. Bull.* **1988**, *23*, 453. (d) Gougeon, P.; Potel, M.; Sergent, M. *Acta Crystallogr.* **1989**, *C45*, 182. (e) Gougeon, P.; Potel, M.; Sergent, M. *Acta Crystallogr.* **1989**, *C45*, 1413. (f) Gougeon, P.; Potel, M.; Sergent, M. *Acta Crystallogr.* **1990**, *C46*, 2284. (g) Thomas, C.; Picard, S.; Gautier, R.; Gougeon, P.; Potel, M. *J. Alloys Compd.* **1997**, *262−263*, 305. (h) Picard, S.; Gougeon, P.; Potel, M. *Acta Crystallogr.* **1997**, *C53*, 1519. (i) Gautier, R.; Picard, S.; Gougeon, P.; Potel, M. *Mater. Res. Bull.* **1999**, *1*, 93. (j) Picard, S.; Potel, M.; Gougeon, P. *Angew. Chem., Int. Ed.* **1999**, *38*, 2034. (k) Picard, S.; Halet, J.-F.; Gougeon, P.; Potel, M. *Inorg. Chem.* **1999**, *38*, 4455. (l) Picard, S.; Saillard, J.-Y.; Gougeon, P.; Noel, H.; Potel, M. *J. Solid State Chem.* **2000**, *155*, 417. (m) Picard, S.; Gougeon, P.; Potel, M. *Acta Crystallogr.* **2001**, *C57*, 335.
(5) Potel, M. Ph.D. Thesis, University of Rennes, 1981.

10.1021/ic020194e CCC: $22.00
Published on Web 08/08/2002

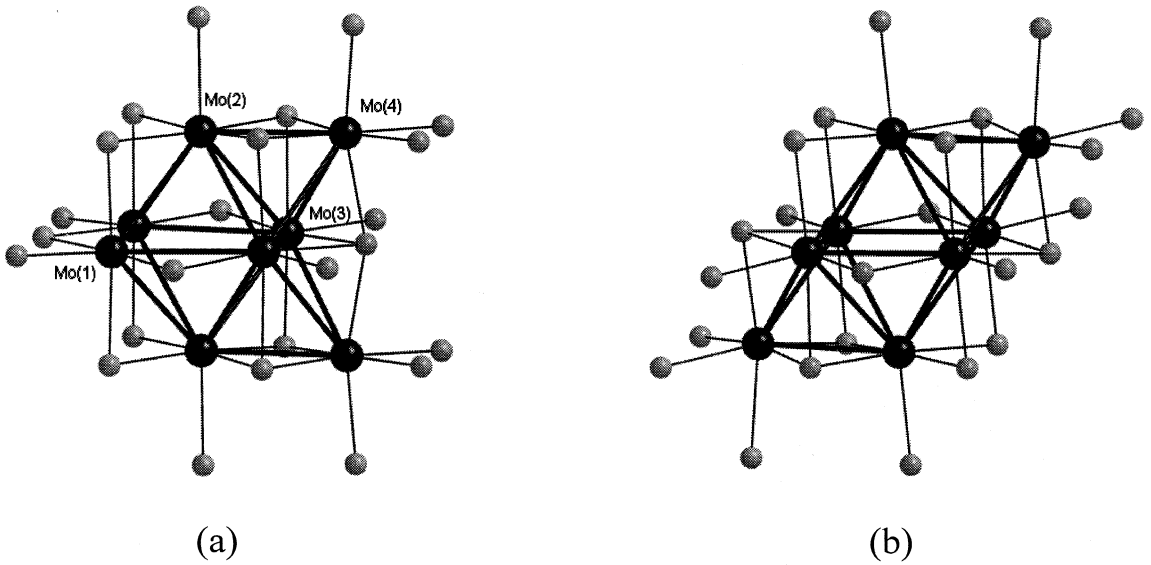

Figure 1. Different *cis* and *trans* bicapped Mo_8O_{24} clusters and their oxygen environment encountered in $LaMo_{7.7}O_{14}$ and RMo_8O_{14} (R = La, Ce, Pr, Nd, Sm) compounds (*trans* Mo_8 motifs were only found for R = La, Ce, Pr).

also observed, Mo_4 clusters exhibit a planar rhomboidal geometry. Clusters with nuclearity larger than six do not result from a one-dimensional *trans*-face sharing of octahedral Mo_6 clusters but rather from a *trans*-edge sharing because of the smaller size of the oxygen atom with respect to the other chalcogens. This leads to an environment in oxygen of the Mo_6X_{12}-type instead of the Mo_6X_8-type as observed with sulfur, selenium, and tellurium atoms. In the former type, the ligands bridge the twelve edges of the Mo_6 octahedron whereas, in the second type, the eight ligand atoms cap each triangular face of the octahedron. In addition, in both cases, six additional ligands are linked to the vertices as terminal ligands to form $Mo_6X_{12}X_6$ and $Mo_6X_8X_6$ units, respectively. The *trans*-edge-sharing condensation process present in oxide systems leads to bi-, tri-, tetra-, and pentaoctahedral Mo_{4n+2} clusters that are observed, for example, in the series $M_{n-x}Mo_{4n+2}O_{6n+4}$ ($n = 2-5$).[6-9] The ultimate step of the edge-sharing-condensation process corresponds to the infinite $|Mo_2Mo_{4/2}|^1_\infty$ chain of *trans*-edge-sharing Mo_6 octahedra that was first observed in $NaMo_4O_6$.[10] In addition to these polyoctahedral Mo_{4n+2} clusters, intermediate clusters, namely Mo_7, Mo_8, Mo_{11}, and Mo_{12} resulting from the Mo capping of one or two faces of octahedral Mo_6 and bioctahedral Mo_{10} clusters, respectively, are also known.[11] The existence of the Mo_7 and Mo_8 clusters was mentioned for the first time by Leligny et al. in the nonstoichiometric compound $LaMo_{7.7}O_{14}$.[12] In fact, starting from the Mo_6O_{18} motif, the Mo_8 cluster can be viewed as resulting from the capping of two adjacent triangular faces by MoO_3 groups (Figure 1a). In $LaMo_{7.7}O_{14}$, the site of the capping molybdenum atom (Mo(4)) is not fully occupied, and one has then to consider the presence of Mo_6 and monocapped Mo_7 clusters. Subsequently, the existence of monocapped Mo_7 clusters was well established in the $M_4M'_3Mo_{26}O_{48}$ (M = Sr, Eu; M′ = Al, Fe, Ga) compounds.[11a] Bicapped Mo_8 clusters were reported in the series of polymorphic compounds RMo_8O_{14} (R = La, Ce, Pr, Nd, Sm), synthesized by solid-state reaction.[13-18] In some of the latter compounds, an isomeric form of the Mo_8 cluster, with the capping MoO_3 groups positioned on opposite faces with respect to the center of the octahedron, is observed (Figure 1b). One can then distinguish these two Mo_8 units as *cis* and *trans* isomers. Prior to the synthesis of the RMo_8O_{14} compounds, no metal mono- or bicapping of a metallic octahedron was observed in any solid-state compound, whereas molecular inorganic chemistry provide several examples such as $Os_7(CO)_{21}$[19] and $[Re_8C(CO)_{24}]^{2-}$.[20] The latter species are richer in electrons than their isostructural solid-state analogues, and their electron count is in agreement with the existing electron-counting rules.[21] Considering in a first approximation the Mo_8 units as isolated motifs because of the rather long Mo−Mo distances separating the cluster units in the RMo_8O_{14} and related compounds, extended Hückel (EH) molecular calculations[22] were first carried out in order to understand

(6) Gall, P.; Gougeon, P. *Acta Crystallogr.* **1993**, *C49*, 659.
(7) Schimek, G. L.; Chen, S. C. *Inorg. Chem.* **1995**, *34*, 6130.
(8) Schimek, G. L.; Nagaki, D. A.; McCarley, R. E. *Inorg. Chem.* **1994**, *33*, 1259.
(9) Dronskowski, R.; Mattausch, H. J.; Simon, A. *Z. Anorg. Allg. Chem.* **1993**, *619*, 1397.
(10) Torardi, C. C.; McCarley, R. E. *J. Am. Chem. Soc.* **1979**, *101*, 3963.
(11) (a) Tortelier, J.; Gougeon, P.; Ramanujachary, K. V.; Greenblatt, M. *Mater. Res. Bull.* **1998**, *33*, 1151. (b) Tortelier, J.; Gougeon, P.; Gautier, R.; Berjoan, R. *Inorg. Chem.* **2001**, *40*, 2292.
(12) Leligny, H.; Ledesert, M.; Labbe, P.; Raveau, B.; McCarroll, W. H. *J. Solid State Chem.* **1990**, *87*, 35.
(13) Gougeon, P.; McCarley, R. E. *Acta Crystallogr.* **1991**, *C47*, 241.
(14) Leligny, H.; Labbe, P.; Ledesert, M.; Raveau, B. *Acta Crystallogr.* **1993**, *B49*, 444.
(15) Kerihuel, G.; Gougeon, P. *Acta Crystallogr.* **1995**, *C51*, 787.
(16) Kerihuel, G.; Gougeon, P. *Acta Crystallogr.* **1995**, *C51*, 1475.
(17) Kerihuel, G.; Tortelier, J.; Gougeon, P. *Acta Crystallogr.* **1996**, *C52*, 2389.
(18) Tortelier, J.; Gougeon, P. *Acta Crystallogr.* **1997**, *C53*, 668.
(19) Eady, C. R.; Johnson, B. F. G.; Lewis, J.; Mason, R.; Hitchcock, P. B.; Thomas, K. M. *J. Chem. Soc., Chem. Commun.* **1977**, 385.
(20) Ciano, P.; D'Alfonso, G.; Freni, M.; Romiti, P.; Sironi, A. *J. Chem. Soc., Chem. Commun.* **1982**, 705.
(21) Mingos, D. M.; Wales, D. J. *Introduction to Cluster Chemistry*; Prentice Hall: New Jersey, 1990.
(22) Hoffmann, R. *J. Chem. Phys.* **1963**, *39*, 1397.

the electronic effect induced by the capping of octahedral Mo_6 clusters, and especially the electronic differences between *cis* and *trans* bicapped Mo_8 clusters.

Physical properties of $LaMo_{7.7}O_{14}$ and the modulated phase $LaMo_8O_{14}$, both prepared by fused salt electrolysis, have already been studied by Ramanujachary et al.[23] We here report electrical and magnetic measurements for the whole series of the RMo_8O_{14} (R = La, Ce, Pr, Nd, Sm) compounds synthesized by solid-state reaction. The main results are described here together with periodic calculations using density functional theory.[24]

Experimental Section

Synthesis. RMo_8O_{14} powders were prepared from a stoichiometric mixture of MoO_3 (Strem Chemicals, 99.9%), Mo (Cime bocuze), and R_2O_3 for R = La, Nd, and Sm (Strem Chemicals, 99.999%). For the Ce and Pr compounds, the starting rare-earth oxides were CeO_2 (Strem Chemicals, 99.999%) and Pr_6O_{11} (Strem Chemicals, 99.9%). Before use, the Mo powder was heated under a hydrogen flow at 1000 °C for 6 h, and the rare-earth oxides were prefired at temperatures between 700 and 1000 °C overnight and left at 600 °C before weighing. The mixtures were pressed into pellets (ca. 5 g) and loaded into molybdenum crucibles which were previously outgassed at about 1500 °C for 15 min under a dynamic vacuum of about 10^{-5} Torr. The Mo crucibles were subsequently sealed under a low argon pressure using an arc welding system. The samples were heated at a rate of 300 °C/h to 1550 °C for 24 h and then cooled at 100 °C/h down to 1100 °C at which point the furnace was shut down and allowed to cool to room temperature. All products were found to be single phase on the basis of their X-ray powder diffraction pattern carried out on an Inel position sensitive detector with a 0−120° 2θ aperture with Cu $K\alpha_1$ radiation. Single crystals were obtained by heating the stoichiometric mixtures to 1950 °C at the rate of 600 °C/h and held there for 10 min followed by cooling at 100 °C/hour down to 1100 °C, at which temperature the power was turned off. Crystals thus formed were typically about $0.1 \times 0.3 \times 0.3$ mm^3 in size.

Electrical Resistivity. Alternating current resistivity measurements were carried out on a single crystal using a standard four-probe technique between 300 and 4.2 K. Ohmic contacts were made by attaching molten indium ultrasonically. The voltage drops across the sample were recorded as a function of temperature. The temperature readings were provided by platinum resistance thermometers.

Magnetic Susceptibility. Magnetic susceptibility data of RMo_8O_{14} (R = La, Ce, Pr, and Nd) were collected on a SHE-906 SQUID magnetosusceptometer in the temperature range 2−300 K under a magnetic field of 4 kGauss. The measurements were carried out on cold pressed powder pellets (ca. 150 mg). Data were corrected from the diamagnetism of the sample holder prior to analysis.

Theoretical Calculations. Extended Hückel[22] molecular calculations were carried out using the program CACAO.[25] The exponents (ζ) and the valence shell ionization potentials (H_{ii} in eV) used were, respectively, 2.275, −32.3 for O 2s; 2.275, −14.8 for O 2p; 1.956, −8.34 for Mo 5s; 1.921, −5.24 for Mo 5p; 2.14. The H_{ii} value for Mo 4d was set equal to −10.50. A linear combination of two Slater-type orbitals of exponents $\zeta_1 = 4.542$ and $\zeta_2 = 1.901$ with equal weighting coefficients was used to represent the Mo 4d atomic orbitals.

Self-consistent ab initio band structure calculations were performed on $LaMo_8O_{14}$[17] and $NdMo_8O_{14}$[13] with the scalar relativistic tight-binding linear muffin-tin orbital (LMTO) method in the atomic spheres approximation including the combined correction.[26] Exchange and correlation were treated in the local density approximation using the von Barth−Hedin local exchange correlation potential.[27] Within the LMTO formalism, interatomic spaces are filled with interstitial spheres. The optimal positions and radii of these additional "empty spheres" were determined by the procedure described in ref 28. Twenty-four and eleven nonsymmetry-related "empty spheres" with $0.59 \le r_{ES} \le 1.37$ and $0.69 \le r_{ES} \le 1.36$ Å were introduced for the calculations on $LaMo_8O_{14}$ and $NdMo_8O_{14}$, respectively. The full LMTO basis set consisted of 6s, 6p, 5d, and 4f functions for La and Nd spheres, 5s, 5p, 4d, and 4f functions for Mo spheres, 2s, 2p, and 3d functions for O spheres, and s, p, and d functions for "empty spheres". The eigenvalue problem was solved using the following minimal basis set obtained from the Löwdin downfolding technique: La and Nd 6s, 5d, 4f, Mo 5s, 5p, 4d, O 2s, 2p and interstitial 1s LMTOs. The k space integration was performed using the tetrahedron method.[29] Charge self-consistency and the average properties were obtained from 8 and 6 irreducible k points for calculations on $LaMo_8O_{14}$[17] and $NdMo_8O_{14}$,[13] respectively.

Table 1. Crystallographic Data of RMo_8O_{14} and Related Compounds

cmpd	space group	a (Å)	b (Å)	c (Å)	isolated cluster ((*cis*-*e*/*trans*) ratio)	ref
$LaMo_{7.7}O_{14}$	*Aba*2	9.196	11.171	9.985	*cis* + Mo_6 + Mo_7	12
$LaMo_8O_{14}$	*Pbcn*	9.2065	11.1298	20.0264	*cis* + *trans* (1/1)	17
$LaMo_8O_{14}$	*Aba*2[a]	9.218	11.129	10.000	*cis* + *trans* (ca. 2/1)	14
$CeMo_8O_{14}$	*Pbcn*	9.1937	11.121	20.014	*cis* + *trans* (1/1)	15
$PrMo_8O_{14}$	*Pbca*	9.2037	11.114	30.012	*cis* + *trans* (2/1)	16
$NdMo_8O_{14}$	*Aba*2	9.209	11.143	10.008	*cis*	13
$SmMo_8O_{14}$	*Aba*2	9.193	11.151	9.997	*cis*	18

[a] Basic space group. This compound exhibits a one-dimensional modulated structure with a modulation vector q^* equal to $c^*/3$.

Results and Discussion

Crystal Structures. The crystal structures of the four crystalline forms in which the RMo_8O_{14} compounds crystallize have been described in detail elsewhere.[12−18] Consequently, only a brief description will be given here. In the four forms (Table 1), the R−O network and the Mo_6 core of the bicapped Mo_8 clusters are similar, differing only in the arrangement of the capping Mo atoms of the Mo_8 clusters. The oxygen sublattice is derived from close-packed layers that are stacked in an ABAC... sequence. In the A layers, a

(23) Ramanujachary, K. V.; Berry Jones, E.; Greenblatt, M.; McCarroll, W. H. *J. Solid State Chem.* **1995**, *117*, 261−268.

(24) (a) Parr, R. G.; Yang, W. *Density Functional Theory of Atoms and Molecules*; Oxford University Press: Oxford, 1989. (b) Jones, R. O.; Gunnarsson, O. *Rev. Mod. Phys.* **1989**, *61*, 689. (c) Kohn, W.; Becke, A. D.; Parr, R. G. *J. Phys. Chem.* **1996**, *100*, 12974. (d) Baerends, E. J.; Gritsenko, O. V. *J. Phys. Chem. A* **1997**, *101*, 5383.

(25) Mealli, C.; Proserpio, D. *J. Chem. Educ.* **1990**, *67*, 399.

(26) (a) Andersen, O. K. *Phys. Rev. B* **1975**, *12*, 3060. (b) Andersen, O. K. *Europhys. News* **1981**, *12*, 4. (c) Andersen, O. K. In *The Electronic Structure Of Complex Systems*; Phariseau, P., Temmerman, W. M., Eds.; Plenum Publishing Corporation: New York, 1984. (d) Andersen, O. K.; Jepsen, O. *Phys. Rev. Lett.* **1984**, *53*, 2571. (e) Andersen, O. K.; Jepsen, O.; Sob, M. In *Electronic Band Structure and its Application*; Yussouf, M., Ed.; Springer-Verlag: Berlin, 1986. (f) Skriver, H. L. *The LMTO Method*; Springer-Verlag: Berlin, 1984.

(27) von Barth, U.; Hedin, L. *J. Phys. C: Solid State Phys.* **1972**, *5*, 1629.

(28) Jepsen, O.; Andersen, O. K. *Z. Phys. B: Condens. Matter* **1995**, *97*, 35.

(29) Blöchl, P. E.; Jepsen, O.; Andersen, O. K. *Phys. Rev. B* **1994**, *49*, 16223.

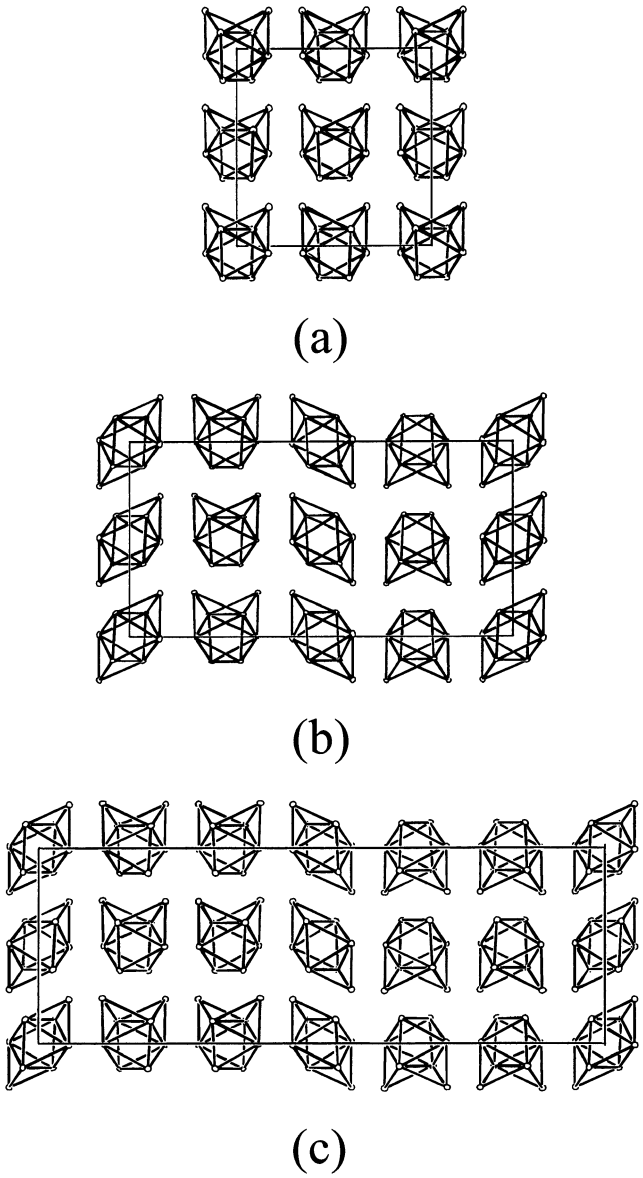

Figure 2. Projections of the metallic networks of the three ordered crystalline forms of RMo_8O_{14} on the (*bc*) plane: (a) $NdMo_8O_{14}$, (b) $LaMo_8O_{14}$, and (c) $PrMo_8O_{14}$.

quarter of the oxygen atoms are missing in an ordered way or substituted by the rare-earth ions. The B and C layers are entirely occupied by oxygen atoms. Within the O network, the Mo atoms occupy half of the octahedral interstices to build the Mo_8 clusters. Figure 2 shows the projections of the Mo network in the (*bc*) plane for the three ordered crystallographic forms. The first crystalline form was observed with the compounds $LaMo_{7.7}O_{14}$, obtained by fused salt electrolysis, and $NdMo_8O_{14}$ and $SmMo_8O_{14}$ were obtained by high-temperature solid-state reaction. These three compounds crystallize in the noncentrosymmetric space group *Aba*2. Their structures only comprise *cis*-edge-sharing bicapped Mo_8 clusters. The other forms show well-ordered mixtures of *cis*-edge-sharing and *trans*-bicapped Mo_8 clusters. Thus, in the La and Ce compounds obtained by high-temperature solid-state reaction, the two isomeric forms of the Mo_8 cluster are encountered in equal proportion while they are in the ratio 2:1 in $PrMo_8O_{14}$. Finally, a modulated form was also discovered with the synthesis of the stoichiometric compound $LaMo_8O_{14}$ by fused salt electrolysis. The crystal structure of the latter compound is more complex because of a one-dimensional commensurate modulation of wavevector $q^* = c^*/3$. The structure that was solved in the superspace group *Aba*2 (00γ) consists of *cis*-edge-sharing and *trans*-bicapped Mo_8 clusters with an average probability distribution of approximately 65% and 35%, respectively. In all the RMo_8O_{14} compounds, the Mo−Mo distances within the Mo_8 clusters range between 2.58 and 2.89 Å. The shortest intercluster distances are about 3.07 Å, and the Mo−O distances range between 1.93 and 2.19 Å as usually observed for the reduced molybdenum oxides. The rare-earth cations are surrounded by 12 oxygen atoms forming a distorted cuboctahedron.

Physical Properties. $NdMo_8O_{14}$ and $SmMo_8O_{14}$ exhibit a quasisimilar and complex semiconducting behavior. Indeed, the log ρ versus $1000/T$ plots shown in Figure 3 show three distinct linear regions, the activation energies of which are 0.04, 0.07, and 0.01 eV in the temperature intervals 80−95, 100−125, and 160−300 K for $NdMo_8O_{14}$, and 0.03, 0.09, and 0.03 eV in the temperature intervals 81−100, 130−150, and 210−300 K for $SmMo_8O_{14}$. The room-temperature resistivities in the (*bc*) plane are 2.0×10^{-3} and 2.2×10^{-3} Ω·cm, respectively. The isostructural molybdenum-deficient compound $LaMo_{7.7}O_{14}$ prepared by fused salt electrolysis also shows a semiconducting behavior with three different thermal activation energies over the temperature range 20−300 K. However, the values of the activation energies differ from those observed for the Nd and Sm congeners, being 0.003, 0.02, and 0.06 eV in the temperature intervals 16−23, 45−105, and 200−280 K, respectively. Its room-temperature resistivity measured in the cluster planes is also slightly higher (5×10^{-3} Ω·cm). $CeMo_8O_{14}$ and $PrMo_8O_{14}$ also show a semiconducting behavior. However, as can be seen from the log ρ versus $1000/T$ plots (see Figure 3), the behavior of the resistivity is less complex with only two linear regions. The activation energies are 0.05 and 0.07 eV in the temperature ranges 65−145 and 180−300 K for $CeMo_8O_{14}$ and 0.04 and 0.07 eV in the temperature intervals 65−145 and 180−300 K for $PrMo_8O_{14}$. The room-temperature resistivities measured in the cluster planes are 2×10^{-3} and 5×10^{-3} Ω·cm for the Ce and Pr compounds, respectively.

The temperature dependences of the molar magnetic susceptibility of $LaMo_8O_{14}$ and of the inverse of the molar magnetic susceptibility of $CeMo_8O_{14}$ and $PrMo_8O_{14}$ are shown in Figure 4. The susceptibility of the La compound is nearly temperature-independent in the range 100−300 K with $\chi_{RT} = 3.4\ 10^{-3}$ emu/mol. This behavior is consistent with the absence of localized moments on the Mo atom network. The low-temperature upturn could be attributed to small amounts of paramagnetic impurities often present in the starting reactants. In contrast, the susceptibility data for the Ce and Pr analogues show a strong temperature dependence (Figure 4) and could be fitted to a modified Curie−Weiss-like behavior in the temperature range 60−300 K. A least-squares fitting of the observed data resulted in a $C =$

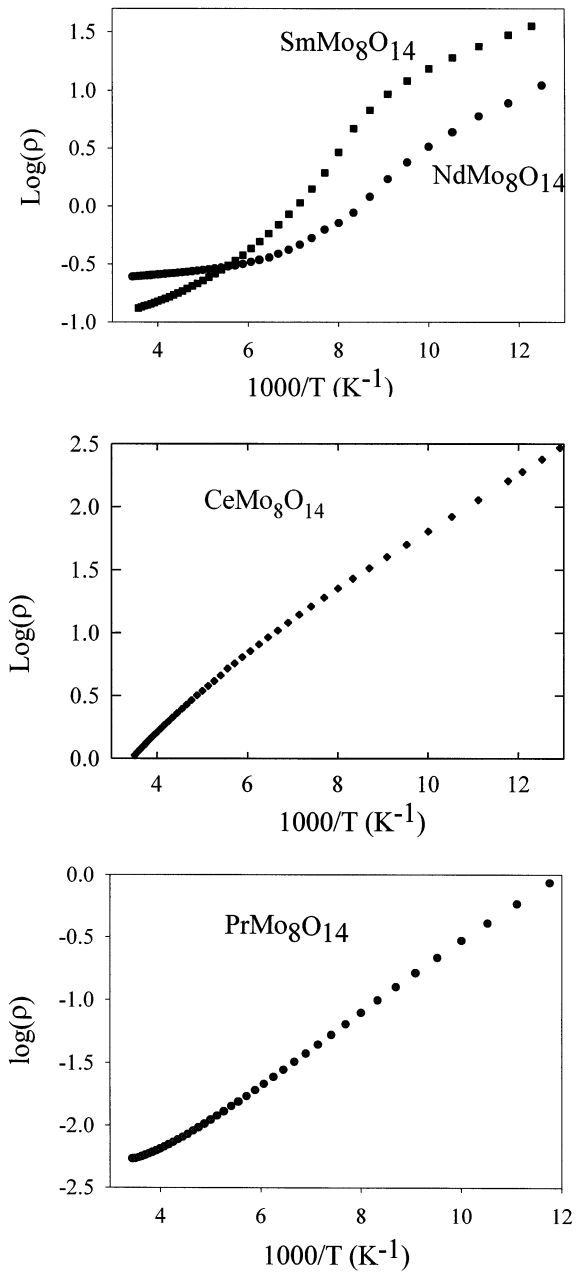

Figure 3. Arrhenius plots for the RMo_8O_{14} (R = Ce, Pr, Sm, and Nd) compounds.

0.783 emu·K/mole, $\theta = -31.8$ K, and $\chi_0 = 2.1 \times 10^{-3}$, and $C = 1.645$ emu·K/mole, $\theta = -19.9$ K, and $\chi_0 = 2.4 \times 10^{-3}$ for the Ce and Pr compounds, respectively. For both compounds, the negative Weiss temperatures suggest that the exchange correlations are antiferromagnetic, although no magnetic ordering was evident down to 2 K. The observed effective magnetic moments ($\mu_{eff} = 2.50\ \mu_B$/Ce and $3.63\ \mu_B$/Pr) are in good agreement with the theoretically expected values of 2.54 and 3.58 μ_B. Figure 5 shows the behavior of the inverse susceptibility with temperature of $NdMo_8O_{14}$. A Curie−Weiss region appears above about 150 K which can be fitted with parameters $C = 1.78$ emu·K/mol and $\theta = -61$ K. The observed Curie constant is somewhat larger than 1.64 emu·K/mol which is the free ion value for Nd^{3+}. This additional contribution may arise, most likely, from the odd

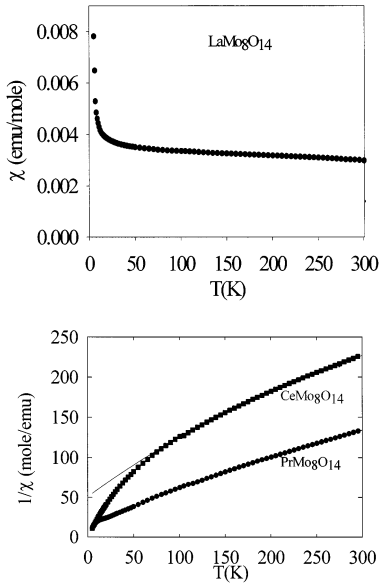

Figure 4. Temperature dependence of the molar magnetic susceptibility of $LaMo_8O_{14}$ and of the inverse of the molar magnetic susceptibility of $CeMo_8O_{14}$ and $PrMo_8O_{14}$. The solid lines correspond to the fit curve.

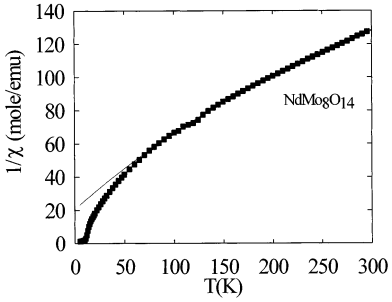

Figure 5. Inverse of the molar magnetic susceptibility of $NdMo_8O_{14}$ vs temperature. The solid lines correspond to the fit curve.

electron cluster, $Mo_8O_{14}^{3-}$ (vide infra). Evidence for long range magnetic order at low temperatures is seen in Figure 6. An inflection point is clearly seen both in χ versus T and $1/\chi$ versus T plots at about 9 K. The shape of the χ versus T curve is characteristic of ferromagnetism or weak ferromagnetism. Isothermal magnetization data at 5 K (Figure 7) show a hysteresis and a rapid rise at low fields to a value near 0.3 μ_B per formula unit, followed by a linear increase with increasing field. These results are also consistent with weak ferromagnetic long range ordering.

Electronic Structure. A plethora of theoretical studies have been devoted to the edge-bridged octahedral cluster of general formula $[(M_6X^i_{12})L^a_6]^{n-}$ (M = Nb, Ta; X^i = two-bonded inner halide ligand; L^a = two-electron donor apical ligand, e.g., H_2O, OH^-, Cl^-, and so forth).[30] These works show that metal electron (ME) counts, that is, the number of electrons available for metal−metal bonding, can vary from 14 to 16 for these arrangements because of a nonbonding (M−M bonding and M−X^i antibonding) molecular orbital (MO) sitting in the middle of a large energy gap

(30) See for example: (a) Hughbanks, T. *Prog. Solid State Chem.* **1989**, 19, 329. (b) Lin, Z.; Williams, I. D. *Polyhedron* **1996**, 15, 3277. (c) Lin, Z.; Fan, M. F. *Struct. Bonding (Berlin)* **1997**, *87*, 35. (d) Ogliaro, F.; Cordier, S.; Halet, J.-F.; Perrin, C.; Saillard, J.-Y.; Sergent, M. *Inorg. Chem.* **1998**, *37*, 6199.

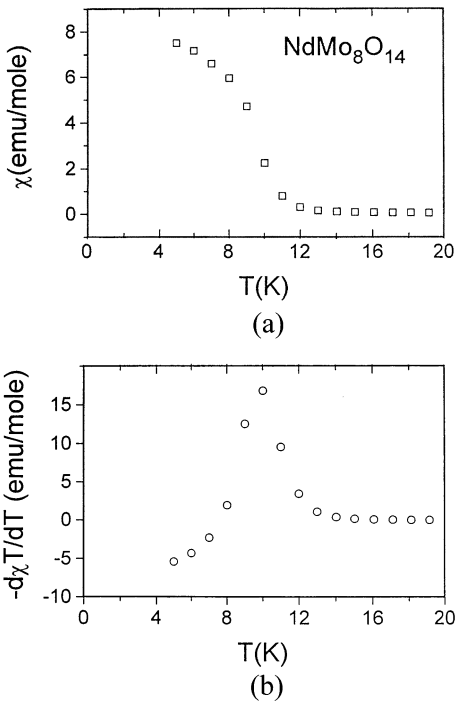

Figure 6. Temperature dependence of the molar magnetic susceptibility (a) and its derivative (b) for $NdMo_8O_{14}$.

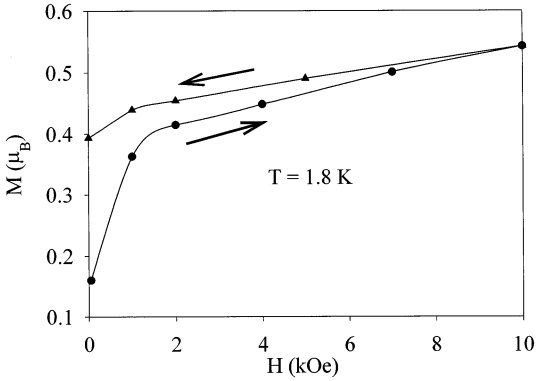

Figure 7. Field dependence of magnetization at 1.8 K for $NdMo_8O_{14}$.

separating a set of M−M bonding MOs from a set of weakly M−M antibonding (M−L nonbonding) MOs. The MO diagram of a $Mo_6O^i_{12}O^a_6$ cluster model of O_h symmetry with Mo−Mo, Mo−O^i, and Mo−O^a distances equal to 2.75, 2.05, and 2.15 Å, respectively, is shown in Figure 8. As expected, an overall nonbonding level of a_{2u} symmetry lies in the middle of a large gap separating 7 MOs of a_{1g}, t_{1u}, and t_{2g} symmetry (shown as a block in Figure 8) which are mainly metal−metal bonding in character, from Mo−Mo antibonding MOs of t_{2g}, e_u, and t_{2u} symmetry. To our knowledge, only two solid-state compounds containing the Mo_6O_{18} motif have been characterized, namely $Ca_{16.5}Mo_{13.5}O_{40}$ and $LaMo_2O_5$.[31,32] The existence of additional Mo atoms (either isolated or in clusters of different shape) in these materials does not allow a precise determination of the electron count of the Mo_6O_{18} units. Nevertheless, estimation of metal

(31) Lindblom, B.; Standberg, R. *Acta Chem. Scand.* **1989**, *43*, 825.
(32) Hibble, S. J.; Cooper, S. P.; Hannon, A. C.; Patat, S.; McCarroll, W. H. *Inorg. Chem.* **1998**, *37*, 6839.

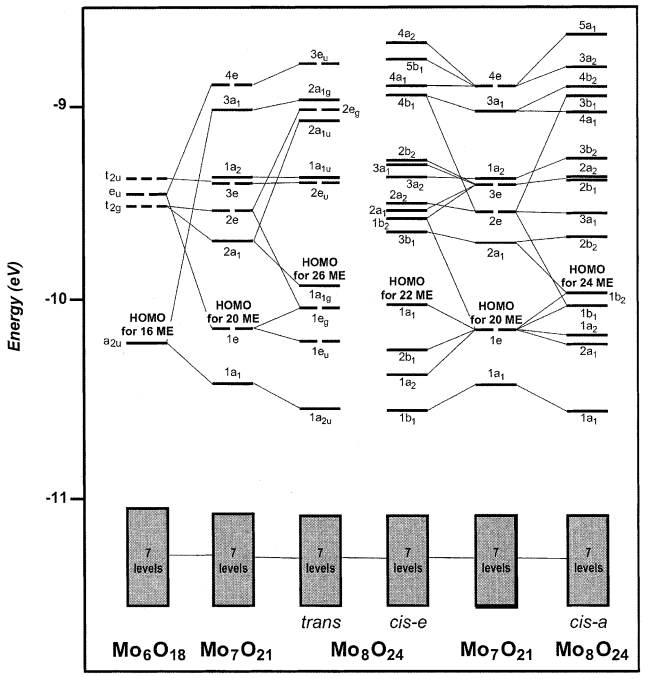

Figure 8. EH molecular orbital diagram of Mo_6, Mo_7, and Mo_8 idealized clusters.

oxidation can be performed on these compounds using the empirical bond length−bond strength relationship proposed by Brown and Wu[33] for Mo−O bonds:

$$s(\text{Mo}-\text{O}) = [d(\text{Mo}-\text{O})/1.882]^{-6}$$

The sum of the Mo−O bond strengths s (in valence units) about a particular Mo atom is equal to the oxidation state of that Mo atom. These calculations lead to an ME count of 16.89 and 16.44 for the Mo_6O_{18} cluster unit in $Ca_{16.5}Mo_{13.5}O_{40}$ and $LaMo_2O_5$, respectively. Indeed, the stoichiometry of the former compound being uncertain, the calculated electron count of 16.89 is probably overestimated so that the real count can be considered to be closer to 16 than 17. The latter count would be unfavorable because of one electron occupying an antibonding MO level (see Figure 8).

The effect of capping a triangular face of a Mo_6O_{18} unit by a MoO_3 fragment is illustrated on the left of Figure 8. The frontier orbitals (FOs) of a MoO_3 fragment of C_{3v} symmetry consist of 3 MOs, one radial hybrid (d_σ) above two tangential hybrids (d_π) with respect to the C_3 axis (of a- and e-type symmetry, respectively). Considering the nodal properties of the occupied a_{1g}, t_{1u}, and t_{2g} MOs of the Mo_6O_{18} cluster (detailed discussions of the nature of these orbitals have already been reported[30] and will not be repeated here), the interaction of the FOs of the capping group with these MOs should be rather weak and negligible in a first approximation. On the other hand, the a_{2u} level which results from a combination of $x^2 - y^2$ orbitals points toward the incoming capping metallic atom (Mo_c vs Mo_o for Mo of the octahedron) and therefore should interact significantly. The MO diagram of an idealized Mo_7O_{21} cluster with C_{3v} symmetry resulting from the interaction from a Mo_6O_{18}

(33) Brown, I. D.; Wu, K. K. *Acta Crystallogr.* **1976**, *B32*, 1957.

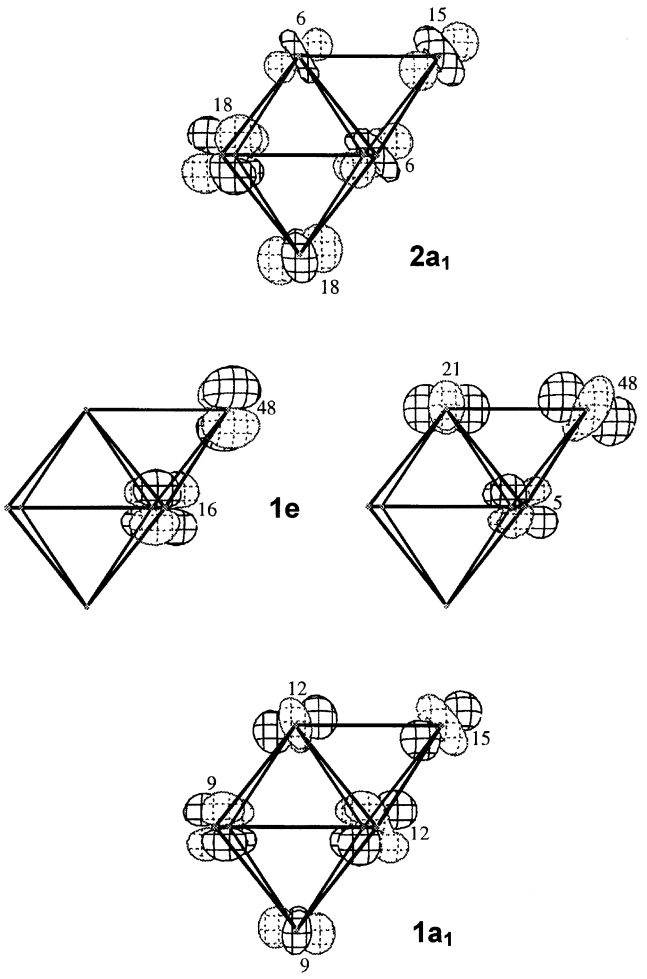

Figure 9. Some frontier molecular orbitals of the Mo_7O_{21} cluster model. Percentages of main atomic contributions are reported.

cluster unit with an MoO_3 fragment confirms this statement (see Figure 8). The strongest interaction between the two fragments occurs between the d_σ orbital of the capping atom and the a_{2u} level of the Mo_6O_{18} unit, leading to the destabilization of the former and the stabilization of the latter (MOs $3a_1$ and $1a_1$, respectively, in Figure 8). Orbital $1a_1$ would lie even lower in energy if it did not mix with one of the 7 levels in the M−M bonding block. The other major interaction involves the pair of tangential hybrids of Mo_c with the high-lying antibonding e_u MO of the octahedral fragment. The resulting bonding combinations lie at rather low energy just above the $1a_1$ combination (see 1e MOs in Figure 8), separated by 0.42 eV from the upper $2a_1$ MO. The sketch of these bonding levels in Figure 9 shows clearly the bonding character between the cluster and the capping atoms. Their occupation leads to a count of 20 MEs for the capped Mo_7O_{21} unit, which maximizes the metal−metal bonding. Simply speaking, the capping of the octahedral cluster leads to the destabilization of the radial orbital of the capping group and the stabilization of the pair of tangential orbitals, increasing by 4 the ME count. This optimal electron count is expected for the isolated Mo_7 unit in $M_4M'_3Mo_{26}O_{48}$ (M = Sr, Eu; M′ = Al, Fe, Ga) compounds.[11a] Empirical bond length−bond strength calculations on these materials, which give a metal electron count of 19.80 for the monocapped Mo_7 octahedral cluster, support our results.

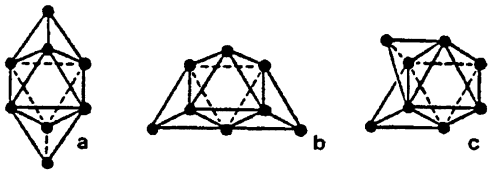

Figure 10. Different isomeric forms of the bicapped M_8 octahedral cluster: *trans* (a); *cis-a* (b); and *cis-e* (c).

With one additional capping MoO_3 fragment, three different bicapped Mo_8 isomeric forms can be envisioned (one *trans* of D_{3d} symmetry and two *cis* of C_{2v} symmetry) (see Figure 10). The two *cis* isomers differ from each other by the capped faces which either share an edge or an apex (hereafter designated by *cis-e* and *cis-a*, respectively). The latter arrangement has only been observed in late-transition metal molecular organometallic chemistry, as exemplified with $[Os_8(CO)_{22}]^{2-}$.[34] The MO diagrams of idealized Mo_8O_{24} clusters with Mo−Mo, Mo−O^i, and Mo−O^a distances equal to 2.75, 2.05, and 2.15 Å, respectively, can conceptually be built from the interaction between the capped octahedral Mo_7 cluster and a capping MoO_3 unit (see Figure 8). For all isomers, the d_σ FO of the MoO_3 fragment interacts mainly with the $1a_1$ MO and one of the seven bonding metallic levels of the Mo_7 unit (see Figure 8). The originally $1a_1$ MO is then weakly stabilized in the three cases, and the d_σ level is destabilized to the empty levels region. Particular care must be taken when considering the energy position of the $1a_{1g}$ MO of the *trans* Mo_8 unit with respect to the other MOs ($3b_1$ in *cis-e* and $2b_2$ in *cis-a*) deriving essentially from the $2a_1$ MO of the Mo_7 fragment. Because of the architecture of the *trans* cluster, the d_σ orbital of the capping group can interact quite strongly with both the $1a_1$ and the $2a_1$ of the Mo_7 cluster in such a way that the $1a_{1g}$ MO is the "nonbonding" combination of a three-orbital pattern, exhibiting some antibonding Mo_o−Mo_c character. This MO lies at particularly low energy because of the involvement in the interaction of the $2a_1$ cluster FO mainly pointing to the *trans* triangular faces of the Mo_7 monocapped octahedron. However, the nature of this orbital is probably easier to understand considering the interaction of the two capping units with the inner octahedral cluster. The radial orbitals of the two capping units lead to two symmetry-adapted orbitals, one of which is stabilized by a metal−metal antibonding cluster orbital but destabilized by a metal−metal bonding cluster orbital leading to the $1a_{1g}$ level, whereas the other is destabilized by a metal−metal bonding cluster orbital leading to an empty orbital of the *trans* Mo_8 unit. Thus, the $1a_{1g}$ orbital incorporates both metal−metal bonding and antibonding contributions of the inner octahedral and capping regions of the cluster. Consequently, from the viewpoint of the metal−metal bonding, this orbital is essentially nonbonding (or very slightly antibonding) and will be quite

(34) Jackson, P. F.; Johnson, B. F. G.; Lewis, J.; Raithby, P. R. *J. Chem. Soc., Chem. Commun.* **1980**, 60.

sensitive to even minor distortions in the metal−metal framework of the cluster. This can lead to variations in the ME count as a function of small changes in the geometry. The tangential MOs of the *trans* capping MoO_3 fragment interact mainly with the 2e MOs and, to a lesser extent, with the 1e MOs of the Mo_7 fragment, giving rise to four low-lying levels ($1e_u$ and $1e_g$ in D_{3d} symmetry). In the *cis-a* isomer, interaction of tangential MOs with FOs of the Mo_7 fragment leads also to the presence of four MO levels ($2a_1$, $1a_2$, $1b_1$, and $1b_2$ in C_{2v} symmetry) at low energy. The *cis-e* model differs from the latter because one of the tangential MOs of the capping fragment shows a significant interaction with the 1e MOs (see Figure 8), and is pushed up in energy. This leads to the presence of only three low-lying MOs ($1a_2$, $2b_1$, and $1a_1$ in C_{2v} symmetry) compared to four in the *cis-a* isomer. In contrast to molecular late-transition metal clusters, the electron count of the bicapped Mo_8O_{24} clusters is strongly dependent on the architecture of the isomer considered. At this point of the discussion, let us note that with our idealized geometries HOMO/LUMO gaps ranging from 0.27 to 0.53 eV are computed for the different clusters with 22 MEs (*cis-e*), 24 MEs (*cis-a*), and 26 MEs (*trans*). These electron counts maximize metal−metal bonding except in the *trans* isomer for which the 24-ME count leads to stronger metal−metal bonding than the 26-ME count (see previous discussion).

The architectures of the Mo_8O_{24} clusters encountered in the solid-state compounds are somewhat distorted with respect to the idealized models described previously. The main features concern a shortening of Mo(1)−Mo(1) and Mo(2)−Mo(4) distances, a lengthening of the Mo(3)−Mo(3) distance in the *cis-e* unit, and a shortening of Mo_c-Mo_o distances in the *trans* cluster. The *trans* and the *cis-e* isomers exhibit very similar bond distances irrespective of the rare-earth element in the RMo_8O_{14} compounds. Empirical bond length−bond strength calculations on these materials lead to ME counts of 22 and 24 for the *cis-e* and *trans* clusters, respectively. Note that the two approaches agree in the ME count for the *cis-e* but differ in that for the *trans* cluster, something which is not that surprising in view of the nature of the $1a_{1g}$ orbital. Considering the relatively small HOMO/LUMO gaps computed for the idealized structures, some second-order Jahn−Teller instability is expected in these models. Indeed, energy is gained upon distortion to the real structures of the *cis-e* and *trans* clusters found in $LaMo_8O_{14}$.[17] This is mainly due to some stabilization of the $1a_1$ MO in the *cis-e* cluster and to some stabilization of the $1e_u$ and $1e_g$ MOs and destabilization of the $1a_{1g}$ MO in the *trans* cluster. Larger HOMO/LUMO gaps of 0.60 and 0.52 eV are computed for the ME counts of 22 and 24 for the *cis-e* and *trans* clusters, respectively. Examination of the metal−metal overlap populations reveals that the maximum Mo−Mo bonding is observed for these peculiar counts. This suggests that any distortion of the idealized C_{2v} architecture of the *cis-a* model might generate a larger energetic gap between bonding and antibonding MOs for the 24-ME count. Our analysis of the dependence of the energy gaps with the detailed structure of the clusters also revealed an additional important feature of the *cis-e* clusters. In that case, the energy of the formally empty $1b_2$ level can substantially change with the position of the oxygen atom that bridges the two capping Mo atoms (see Figure 1). As it can be easily understood, interaction with the p_z orbital of the bridging oxygen atom destabilizes the antisymmetric combination of one of the two tangential orbitals of the capping groups in the *cis-e* cluster. Thus, the energy of the $1b_2$ level will strongly depend on the Mo_c-O distance. Of course, such destabilization cannot occur in the *cis-a* cluster. Whereas in the case of the *cis-a* clusters only one ME count (24) is to be expected, in *cis-e* clusters there can be some adaptability to the structural details (i.e., ME counts between 22 and 24 could be possible). For instance, when the structure found in $NdMo_8O_{14}$[13] was used for the *cis-e* cluster, the $1b_2$ level was found to be considerably stabilized so that it could well be filled with additional electrons. Consequently, we conclude that both the *cis-e* and *trans* clusters can exhibit a remarkable ME count adaptability.

At this point, it is useful to consider the ME counts which can be estimated from the data in Table 1 (we are reminded that all *cis* clusters observed to date are of the *cis-e* type). Assuming the usual oxidation state of +3 for the lanthanide atoms, the ME count for the *cis-e* clusters in $SmMo_8O_{14}$ and $NdMo_8O_{14}$ should be 23. Taking into account the ratio between the *cis-e* and *trans* clusters, the minimum ME counts for the *cis-e* and *trans* clusters of $PrMo_8O_{14}$ and the $LaMo_8O_{14}$ compound reported in ref 14 should be 22 and 25, respectively. For $CeMo_8O_{14}$ and the $LaMo_8O_{14}$ given in ref 17, the ME counts should be 22 and 24, respectively. These observations fit very nicely with the previous analysis. It is also interesting to consider the incommensurately modulated phase reported for $LaMo_{7.7}O_{14}$.[12] On the basis of the stoichiometry (i.e., occupation of 85% of the capping Mo position), Leligny et al.[12] proposed two structural alternatives for this phase. In the first one, 85% of the clusters were of the *cis-e* type, and the 15% remaining were simply octahedral ones. In the second, 70% of the clusters were of the *cis-e* type, and 30% were randomly occupied monocapped clusters. These two possibilities are equally correct from a strictly structural viewpoint. Our theoretical analysis allows a more in-depth discussion of the likeliness of these structural alternatives. On the basis of the minimum ME counts, required for metal−metal bonding, of 16 MEs per octahedron, 20 ME per monocapped cluster, and 22 MEs per *cis-e* cluster, the average ME count per formula unit should be 21.1 ($0.85 \times 22 + 0.15 \times 16$) in the first case and 21.4 ($0.7 \times 22 + 0.3 \times 20$) in the second. These values are respectively slightly lower and higher than the value of 21.2 based on the observed stoichiometry. Thus, an additional 10 electrons per 100 formula units are required for the 85% *cis-e*/15% octahedra model, whereas 30 electrons per 100 formula units must be removed from the required ME count to accommodate the model with 70% *cis-e*/30% monocapped clusters. Given that the orbitals immediately above the HOMO in the capped clusters are essentially nonbonding cluster orbitals, it is preferable to add a few electrons to nonbonding orbitals than to remove electrons from the metal−metal bonding orbitals. A third possibility, intermedi-

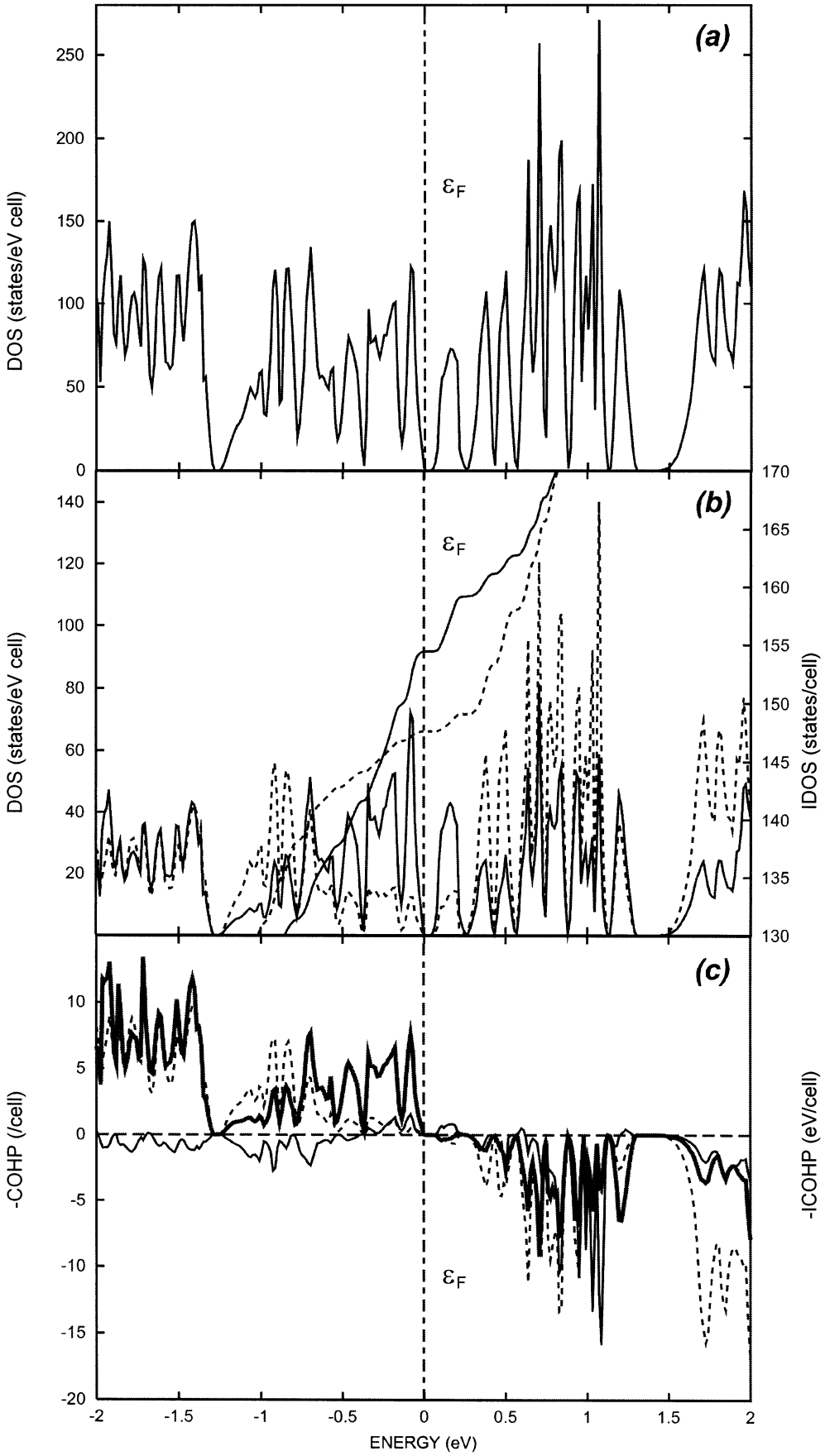

Figure 11. (a) Total DOS of $LaMo_8O_{14}$. (b) *trans* (−) and *cis-e* (- - -) Mo_8 projected DOS. (c) Intra *trans* Mo_8 (−), intra *cis-e* Mo_8 (- - -), and intercluster (−) Mo−Mo COHP.

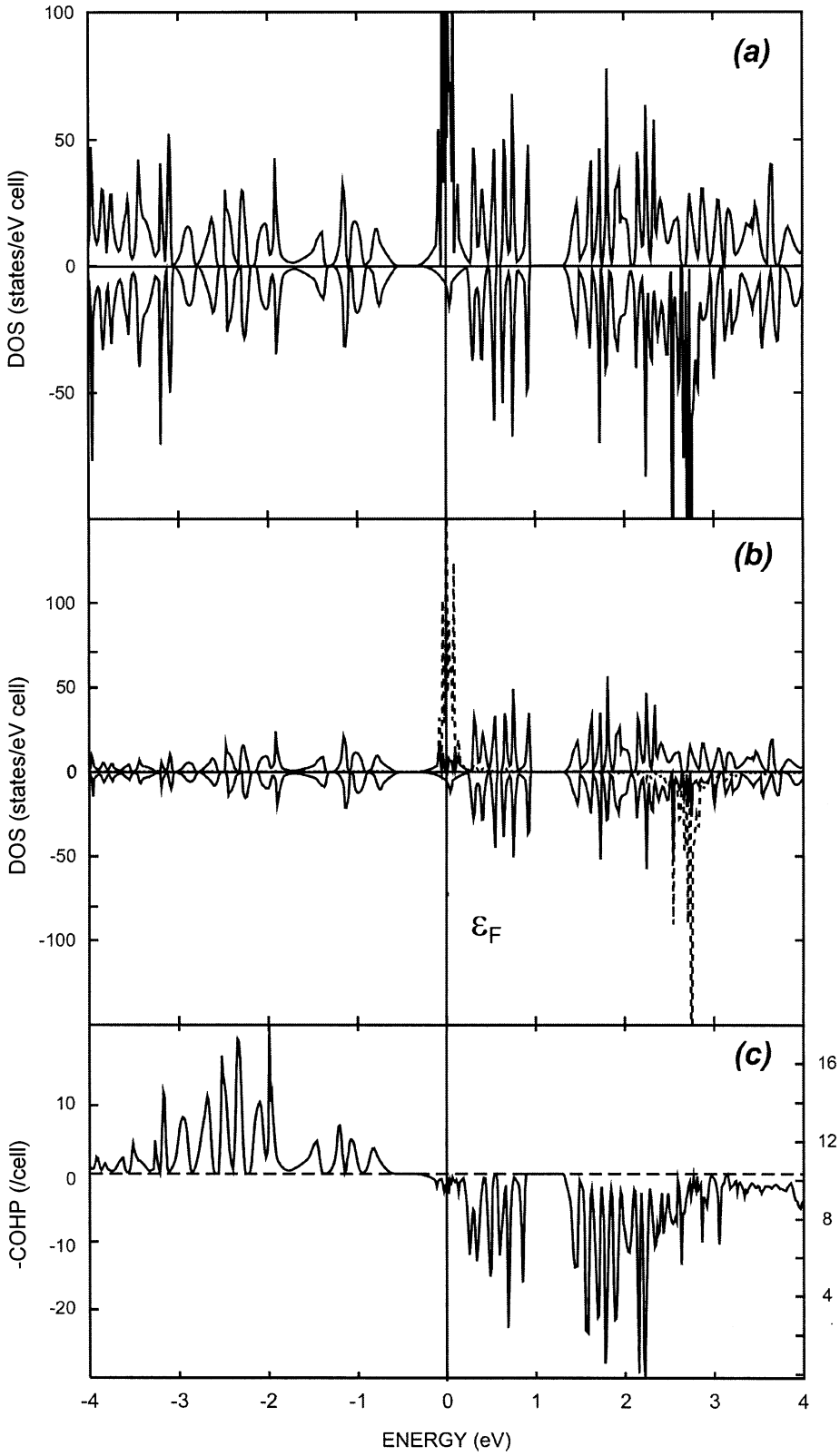

Figure 12. (a) Spin-polarized total DOS of $NdMo_8O_{14}$. (b) Nd (- - -) and Mo (−) projected DOS. (c) Intra *cis-e* Mo_8 Mo−Mo COHP.

ate between the previous two, in which 80% of the clusters are of the *cis-e* type, 10% are simply octahedral, and 10% are monocapped clusters ($0.8 \times 22 + 0.10 \times 16 + 0.10 \times 20$), leads to the observed ME count of 21.2 ME. Magnetic susceptibility measurements would differentiate this latter closed shell model from the previous two that should exhibit a small paramagnetic moment.

The electronic structure of these bicapped octahedral Mo_8O_{24} units is distinctly different from that of the isostructural organometallic analogues. In the latter, high-lying

FOs of the capping group strongly interact with occupied orbitals of the parent octahedral cluster in such a way that the number of electrons responsible for the metal−metal bonding remains unchanged.[21] This is the classic result of a two-orbital, two-electron interaction in which bonding and antibonding MOs are formed, but only the bonding orbital is filled, thus resulting in no net gain in the total electron count. By contrast, in the relatively early-transition metal Mo_6O_{18} clusters, the Mo t_{2g}-type orbitals form both the M−M bonding orbitals as well as a block of weakly antibonding (effectively nonbonding) orbitals (t_{2g}, e_u, and t_{2u}) which are higher in energy than the orbitals of the capping fragment. The M−M bonding orbitals, the orbitals of the capping fragment, and these nonbonding orbitals set up a classic three-center interaction resulting in bonding, nonbonding, and antibonding combinations. If only the bonding combinations are occupied then there is no net addition to the ME count. However, occupation of the intermediate nonbonding levels (weakly cap-to-cluster bonding) adds to the total ME count

Ab initio periodic calculations using the TB-LMTO-ASA method[24] were carried out on $LaMo_8O_{14}$[17] and $NdMo_8O_{14}$[13] in order to evaluate the perturbation of the Mo_8 clusters' MO patterns in the three-dimensional solids. Several crystal overlap Hamiltonian population (COHP) curves indicating energetic contribution of crystal orbitals between orbitals and/or atoms,[26] and density of states (DOS) curves were computed. Calculations on the $LaMo_8O_{14}$ phase confirm the nonmagnetic and semiconducting properties of this compound with a small energy gap of 0.05 eV separating the valence band from the conduction band (see Figure 11). This value compares well with that computed for the isostructural compound $CeMo_8O_{14}$. Analyses of the occupied bands at the Fermi level, atomic charges, and intra-Mo_8 COHP curves show that the band structure of $LaMo_8O_{14}$ consists of narrow peaks of DOS resulting from the superposition of bands deriving from *cis-e* and *trans* Mo_8 cluster levels. This indicates that intercluster interactions must be rather weak. While the shortest intercluster contacts are between the capping fragment of one cluster to the body of the neighbor, the MOs tend to be localized on either the cap or the cluster, thus giving rise to no significant intercluster overlap. Indeed, COHP curves shown in Figure 11 indicate that the intercluster Mo−Mo bonding is 10 times weaker than Mo−Mo bonding in the Mo_8 cluster (−0.010 Ry/cell vs −0.101 Ry/cell (averaged)). This suggests that these compounds are highly molecular in character. The difference in the ME count for the *cis-e* and *trans* Mo_8 clusters in the $LaMo_8O_{14}$ compound is illustrated by the integrated DOS curves.

Spin-polarized calculations on $NdMo_8O_{14}$[13] were also carried out. The Fermi level for the observed electron count crosses an important and narrow DOS peak which is mainly Nd 4f in character (see Figure 12). This peak is separated by an energy gap of 0.20 eV from Mo peaks deriving from the Mo_8 clusters. This band gap is the corresponding HOMO/LUMO gap of the *cis-e* Mo_8 cluster for 22 MEs. It separates Mo−Mo bonding and nonbonding bands from antibonding bands of the Mo_8 unit (see COHP curve c in Figure 12). As shown in Figure 12, the filled part above the energy gap is weakly Mo−Mo energetically unfavorable, something which stems from partial occupation of the b_2 levels for the reasons outlined previously. This rationalizes the observation of a 23-ME count for this phase instead of the more common 22-ME count. As in $LaMo_8O_{14}$, Mo−Mo intercluster COHP curves reveal weak interactions between Mo_8 units, in agreement with the semiconducting properties measured for $NdMo_8O_{14}$. The magnetic moment computed for Nd^{3+} in $NdMo_8O_{14}$ is higher than that expected for the free ion. This is due to additional contributions coming from the molybdenum atoms which bear significant spin density.

Conclusion

Electrical and magnetic properties were measured for the RMo_8O_{14} compounds (R = La, Ce, Pr, Nd, Sm). Semiconducting behavior is found for the whole series. Theoretical calculations were carried out in order to understand the bonding mode in these materials. Results indicate that both the *cis-e* and *trans* clusters can modulate the optimal ME count as a function of weak structural readjustments. These compounds are highly molecular in character, consisting of nearly isolated bicapped octahedral 22-ME *cis-e* and 24-ME *trans* Mo_8 cluster units in $LaMo_8O_{14}$[17] and 23-ME *cis-e* Mo_8 cluster units in $NdMo_8O_{14}$.[13] In contrast to capped organometallic cluster compounds, metal electron increasing is observed for capped molybdenum−oxygen octahedral clusters with respect to the octahedral parent derivatives.

Acknowledgment. R.G. thanks the Max-Planck-Gesellschaft (Germany) and the Centre National de la Recherche Scientifique (France) for a postdoctoral grant. This work was partially supported (E.C.) by DGI-Spain (Project BFM2000-1312-C02-01) and Generalitat de Catalunya (Project 1999 SGR 207).

IC020194E